United States
Naval Postgraduate School

THESIS

THE EXPERIMENTAL DESIGN AND OPERATION

OF A ROTATING WICKLESS HEAT PIPE

by

Thomas James Daley

June 1970

60

THE EXPERIMENTAL DESIGN AND OPERATION OF A ROTATING WICKLESS HEAT PIPE

by

Thomas James Daley
Lieutenant, Junior Grade, United States Navy
B.S., United States Naval Academy, 1969

Submitted in partial fulfillment of the
requirements for the degree of

MASTER OF SCIENCE IN MECHANICAL ENGINEERING

from the

NAVAL POSTGRADUATE SCHOOL
June 1970

Author Thomas J. Daley

Approved by: Paul J. Marto
Thesis Advisor

Chairman, Department of Mechanical Engineering

R. J. Rinehart
Academic Dean

ABSTRACT

An experimental rotating wickless heat pipe apparatus was designed and machined. The apparatus includes a rotating heat pipe assembly, test stand, spray cooling assembly, safety shielding, and instrumentation.

A revised condensing limit for the operation of the rotating heat pipe was obtained by modifying Ballback's Nusselt film condensation theory to include the effects of a thermal resistance in the condenser wall and in the condenser outside surface cooling mechanism. Approximate results, obtained for half-cone angles of 1, 2, and 3 degrees, show that less heat can be removed than originally predicted by Ballback[7], and that the outside heat transfer coefficient can significantly alter the condensing limit.

An improved Nusselt theory was developed which applies for all half-cone angles, and which includes the effects of the thermal resistances in the condenser wall and in the condenser outside surface cooling mechanism. This formulation led to a second-order non-linear differential equation for the film thickness which was numerically integrated using a free-overfall boundary condition at the condenser exit. Results obtained for a half-cone angle of 0 degrees are substantially less than the results obtained from the approximate solution for half-cone angles of 1, 2, and 3 degrees.

TABLE OF CONTENTS

LIST OF ILLUSTRATIONS

LIST OF SYMBOLS

A	area, ft^2
A_b	evaporator inside surface area, ft^2
C	coefficient of Reynolds Number in analysis for Nusselt Number
c	Chezy constant, $\sqrt{ft}/hr$
h	condenser outside surface convection coefficient, $Btu/hr\text{-}ft^2\text{-}^oF$
h_{fg}	latent heat of vaporization of working fluid, Btu/lbm
I	current, amperes
k	thermal conductivity, $Btu/hr\text{-}ft\text{-}^oF$
L	length, ft
m	exponent of Reynolds Number in analysis for Nusselt Number
$\dot{m}_f$	condensate mass flow rate, lbm/hr
P	electrical power, watts
Q	heat transfer rate, Btu/hr
q	heat flux, $Btu/hr\text{-}ft^2$
R	electrical resistance, ohms
R	thermal resistance, $^oF\text{-}hr\text{-}ft/Btu$
R	radius of evaporator inside surface, ft
R_o	minimum wall radius in condenser section, ft
r	radial direction, ft
r'	radius of thermocouple embedded in evaporator wall, ft
S_f	friction slope
S_o	bed slope
T	temperature, ^oF
t	condenser wall thickness, ft
X	coordinate direction along condenser wall, ft

Y	coordinate direction normal to condenser wall, ft
δ	condensate film thickness, ft
ρ	density, lbm/ft^3
μ	dynamic viscosity, ft^2/hr
ω	rotational speed, 1/hr
ϕ	condenser half-cone angle, rad

subscripts

b	boiler
c	overfall
f	fluid
inc	inconel
inf	ambient
ins	insulation
i	inside
MgO	magnesium oxide
o	outside
s	saturation
ss	stainless-steel
w	condenser wall

ACKNOWLEDGEMENTS

The author would like to express his appreciation to Dr. P. J. Marto of the Naval Postgraduate School for his advice and constructive criticisms of this study as thesis advisor, and to Dr. M. D. Kelleher as departmental reader. Special thanks are due to Michael O'Day and Don Harvey at the Postgraduate School Machine Shop for the outstanding job they did on the machining of the heat pipe.

This work was performed under NASA Defense Purchase Request W-13,007 for the Lewis Research Center, Cleveland, Ohio.

B L A N K

I. INTRODUCTION

A. CONVENTIONAL HEAT PIPE

A heat pipe is a self-contained device capable of transporting large quantities of heat at nearly isothermal conditions. Conventionally it consists of three main parts: a container, a working fluid, and a wicking structure capable of promoting capillary action.

When heat is added to one end of the container, some of the working fluid evaporates. This end is the evaporator. The pressure differential in the vapor chamber due to the increase in vapor at the evaporator causes the vapor to flow to the opposite end of the container, transporting heat as latent heat of vaporization. Here the vapor condenses on the cooler surface and releases the heat to be removed from the structure. This end of the container becomes the condenser. The condensate is pumped back to the evaporator section by capillary action, thus completing the cycle. The heat pipe is unique in that it operates with no moving parts, maintains nearly isothermal conditions, and removes the dependency on gravity through the use of capillary pumping.

Limits on the heat transfer capabilities of conventional heat pipes are imposed by a number of fluid dynamic mechanisms; including a wick resistance limit, a sonic vapor velocity limit, a vapor velocity entrainment limit, and also a wick boiling limit. These limits have been considered in a number of studies [1, 2, 3, 4]* with the conclusion that in general a conventional heat pipe using an ordinary working fluid is limited by the rate that the condensate can be returned to the evaporator due to wick resistance.

* Numbers in brackets indicate references listed in Bibliography.

B. THE ROTATING, WICKLESS HEAT PIPE

The restriction imposed by the inability of the wicking structure to provide sufficient pumping force to return condensate to the evaporator can be alleviated by removing the wick and utilizing centrifugal acceleration as a pumping source [5]. If the pipe is allowed to rotate about its longitudinal axis and the wall is given a slight taper, a rotational force field can easily be produced that not only overcomes the viscous losses in the system, but also the losses due to a hindering gravitational field. The operation of a rotating heat pipe is shown schematically in FIGURE 1.

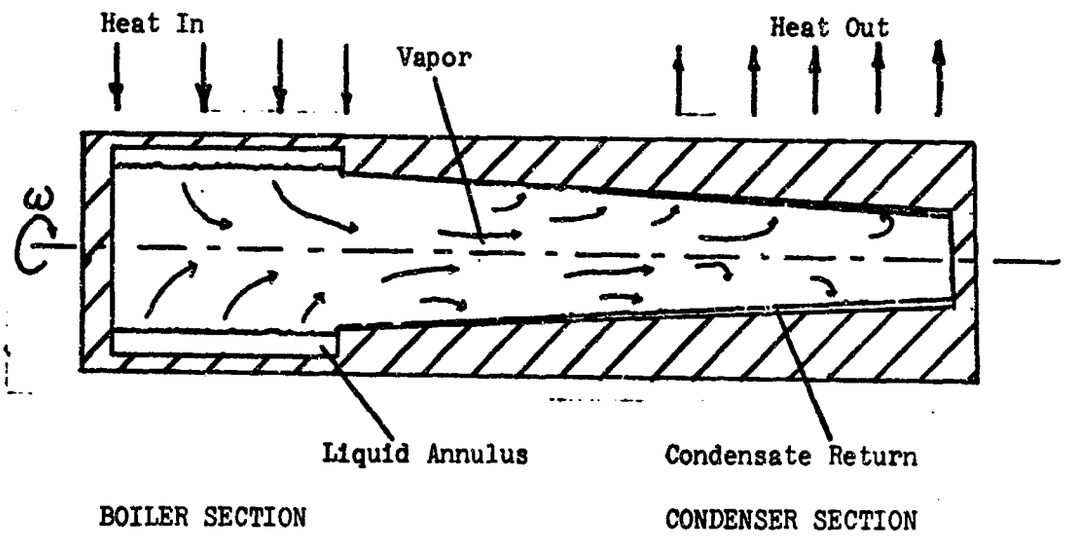

FIGURE 1. Schematic Drawing of Typical Rotating Heat Pipe

The applications of a rotating heat pipe appear to be wide and varied. Wherever there is rotation and a need to transfer heat, the use of such a system is feasible. The cooling of motor rotors, turbine rotor blades, aircraft braking systems, and air-conditioning units are just a few examples of the uses to which the rotating heat pipe concept can be applied.

The capillarity of the wicking structure need no longer be considered as a limit on heat pipe operation since it has been replaced as a pumping force by an artificial gravity head. Ballback [7] has studied the limitations imposed on the rotating system by various fluid dynamic mechanisms in a preliminary theoretical analysis of the operation of a wickless heat pipe. By using existing theories and experimental correlations, he was able to estimate the limits on rotating heat pipe operation imposed by the onset of critical nucleate boiling, condensate entrainment, and choked vapor flow. An estimate of a condensing limit was obtained by performing a Nusselt-type analysis for condensation on a truncated cone, since existing theory and correlations were not applicable. This analysis, however, was restricted by certain simplifying assumptions that were made to obtain a closed-form analytical result. Ballback's results indicated that the operation of a rotating heat pipe is limited by the amount of heat that can be removed from the condenser section.

C. THESIS OBJECTIVES

The objectives of this study were to: a.) design and construct an experimental rotating heat pipe assembly; b.) revise and supplement the initial theoretical study of rotating heat pipe operation performed by Ballback.

II. EXPERIMENTAL PROGRAM

A. BASIC DESIGN CONCEPTS

For Ballback to generate numerical results from his theoretical model, a fixed geometry for the heat pipe had to be decided upon. He chose to model the evaporator section along the lines of the rotating boiler used at the Lewis Research Center in Cleveland, Ohio, for the study of boiling heat-transfer coefficients operating under high gravity levels [6]. With this geometry fixed he allowed the size of his condenser section (length and base radius) to be governed by the amount of taper in the section. The taper was defined by the half-cone angle, which was a parameter in the theoretical study. A strong influence in the overall design was the desire to be able to visually observe the mechanisms that were taking place within the heat pipe during operation. The onset of critical nucleate boiling and the entrainment of the returning condensate were two principal phenomena which were to be observed.

B. DESCRIPTION OF EQUIPMENT

The components of the wickless heat pipe are divided into four sub-groups to simplify the explanation of their design and construction. These are: 1.) evaporator 2.) condenser, 3.) auxiliary equipment, and 4.) instrumentation. FIGURE 2 is a schematic representation of all the components of the test apparatus. A cross-sectional drawing of the assembled heat pipe is pictured in FIGURE 3 and FIGURE 4 is a photograph of the machined pieces of the rotating heat pipe prior to assembly.

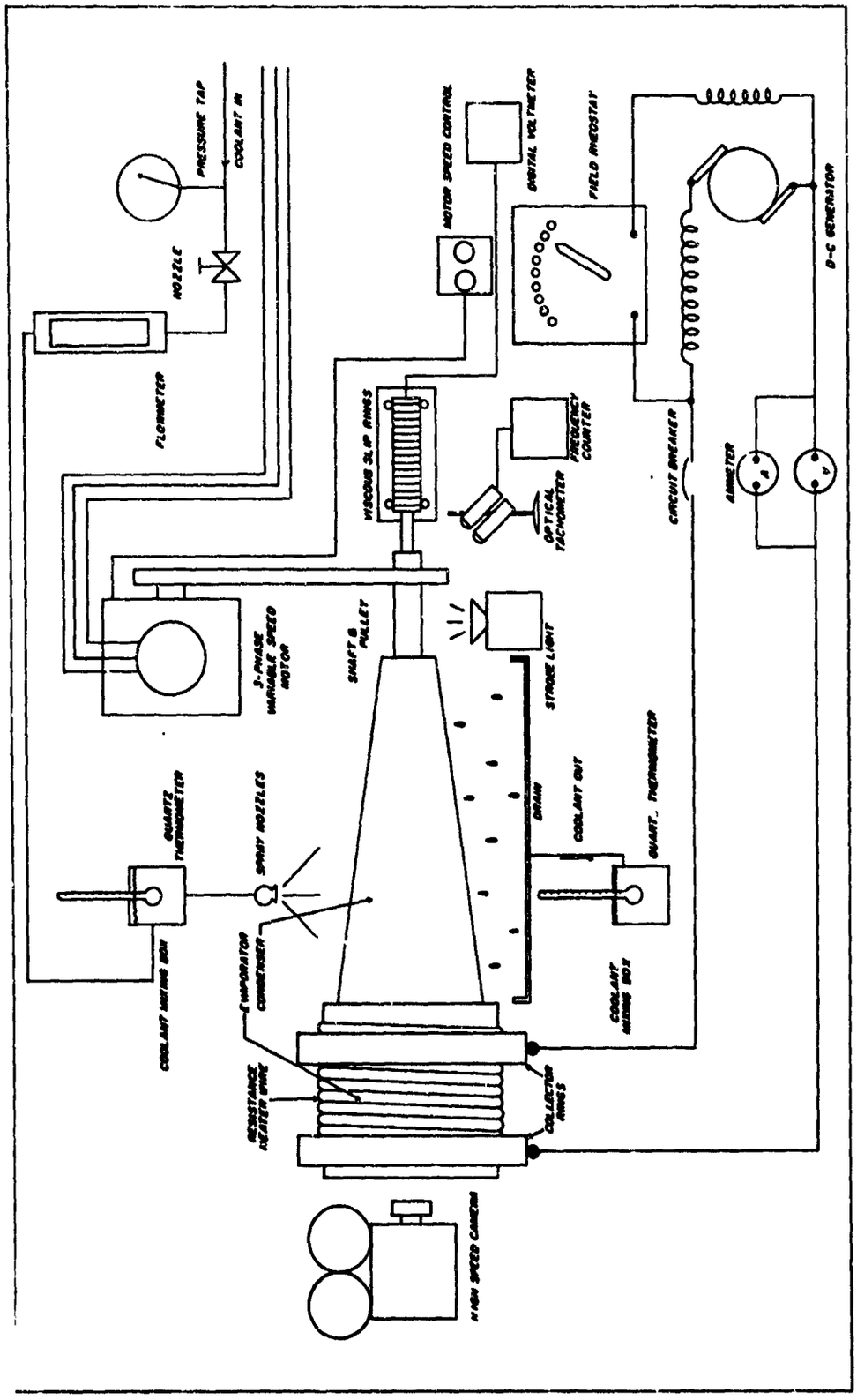

FIGURE 2 SCHEMATIC DIAGRAM OF APPARATUS

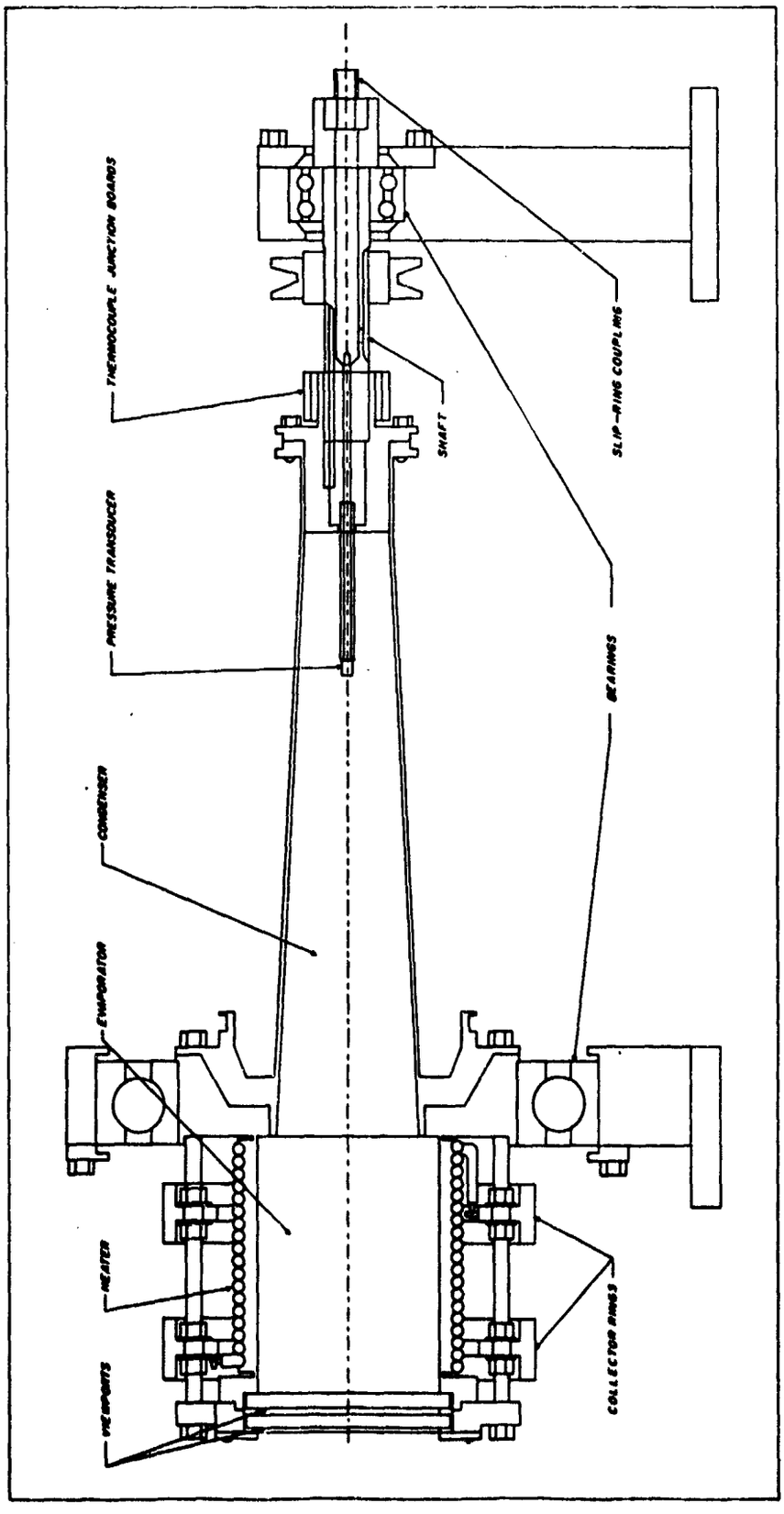

FIGURE 3 CROSS SECTION OF ROTATING HEAT PIPE

FIGURE 4 Machined Rotating Heat Pipe Prior to Assembly

1.) The Evaporator

The evaporator was modeled to approximate the rotating boiler tested at Lewis Research Center [6] . It was machined of stainless-steel because of this metal's corrosion-resistant properties. It has an inside diameter of 3.125-inches, an exit diameter of 2.625-inches, and an overall length of 5.905-inches (see FIGURE 3). This length includes 2/3-inch for the insertion of two pyrex-glass viewports, 4-inches of heating surface, and an intended $\frac{1}{2}$-inch adiabatic section. The inside diameter of the evaporator is stepped $\frac{1}{2}$-inch from the exit diameter to allow for the formation of a liquid annulus. The inner viewport rests on a teflon-coated metallic O-ring seal and is separated from the outer viewport by a 3/32-inch thick compressed-fiber gasket. The viewports are held in place by a stainless-steel end cap which is secured in place by twelve $\frac{1}{4}$-inch stud-bolts. These bolts also support two bronze collector rings. The rings are insulated from their supports by 1/16-inch teflon tubing and washers. Electrical power is passed by a brush assembly consisting of eight spring-loaded graphite brushes through the collector rings to an 11-gage Chromel-A heater wire in a 3/16-inch inconel sheath. Power to the heater is furnished by a DC motor-generator capable of delivering 150 amperes at 220 volts. The heater was helically wound and silver-soldered in place to insure good thermal contact. After the heater was coated with a thin layer of Sauereisen cement, asbestos insulation was packed around the outside to reduce the radial heat losses. In addition two radial 1/16-inch grooves were machined on the outside surface to within 1/16-inch of the inside boiler wall at either end of the heating element to lessen axial heat losses.

With this construction and by assuming a maximum operating temperature for the heater element, it is possible to estimate the maximum heat flux into the boiler. Likewise, it is possible to estimate the heat losses by approximating the outside convection coefficient from an analysis of air flow over a stationary cylinder [11]. These calculations are shown in Appendix A. The results indicate that a maximum radial heat flux of approximately 470,000 Btu/hr-ft^2 can be obtained with an associated radial heat loss of approximately 1300 Btu/hr-ft^2 (with 3/4-inch asbestos insulation).

As noted in Appendix A, the heat flux is dependent upon the thermal resistances that lie in the radial heat transfer path. The dominant resistance is that of the stainless-steel evaporator wall because of its low thermal conductivity. It is therefore advantageous to keep the thickness of the wall as small as possible. However, as mentioned in the section on instrumentation, thermocouples are to be imbedded in the boiler wall to monitor the temperature to obtain a temperature gradient and associated heat flux. From an uncertainty analysis (Appendix B), it is found that the farther apart the thermocouples are radially mounted to one another, the smaller the uncertainty in determining an accurate heat flux. So there is a trade-off on the selection of the wall thickness. In this case, a thickness of $\frac{1}{8}$-inch was used.

A photograph of the machined evaporator section is shown in FIGURE 5.

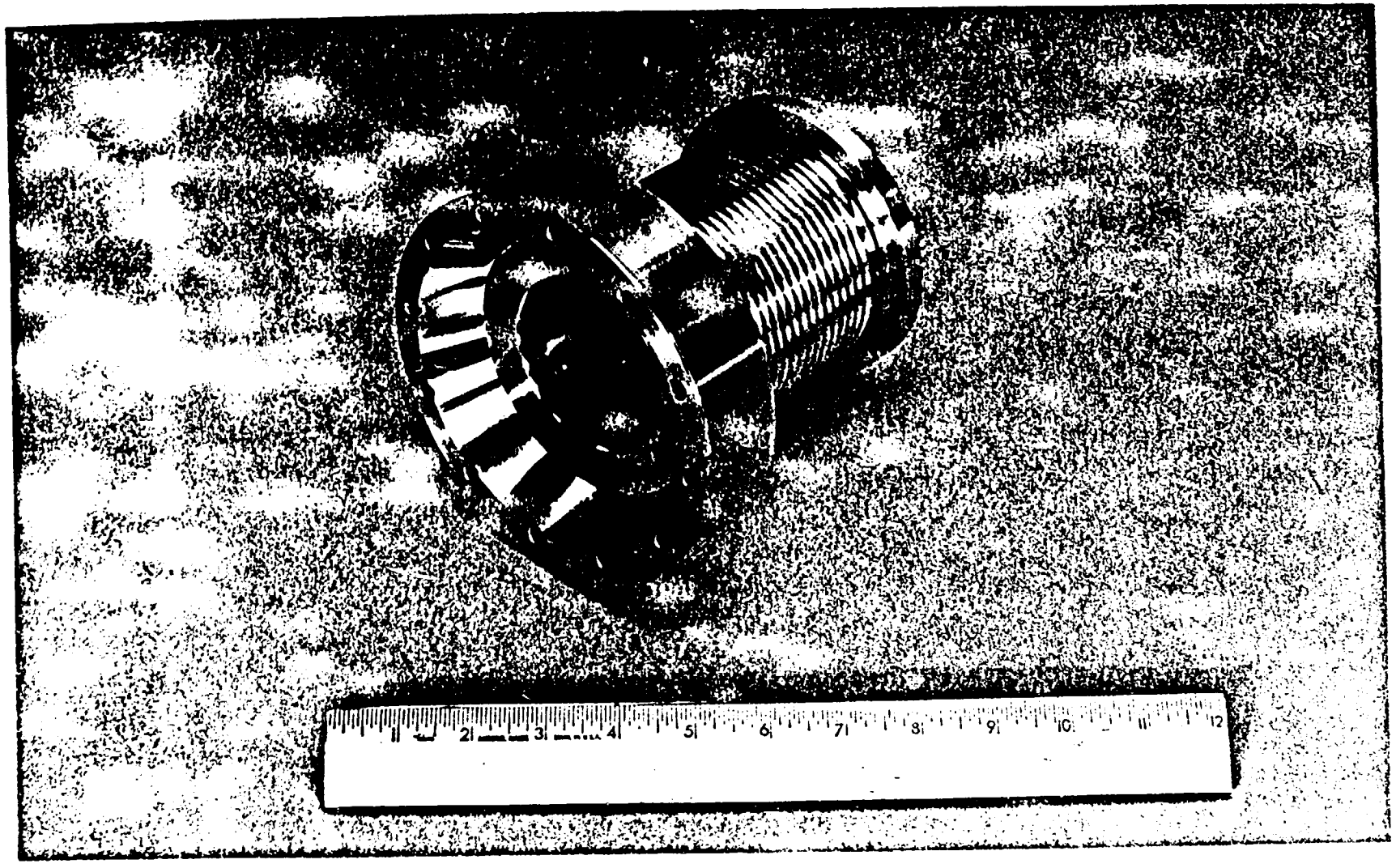

FIGURE 5 Machined Evaporator Section

2.) The Condenser

The condenser section was machined of stainless-steel in the shape of a truncated cone with a 3 degree half-cone angle. The base of the condenser mates to the evaporator exit and has an inside diameter of 2.5-inches (see FIGURE 3). A step is created at the evaporator-condenser intersection where the condensate flows from the condenser to the recessed inside diameter of the evaporator. The condenser tapers from an inside diameter of 2.5-inches to one of 1.46-inches at the truncated end over a length of 10-inches. From here the condenser extends an additional 1 1/2-inches to house a cylindrical end plug. Of the overall length, 9-inches (along the axis) is considered to be the cooling surface. The first inch of the condenser surface near the evaporator is assumed to be adiabatic. The wall thickness of the condenser is 1/16-inch to keep the thermal resistance as small as possible.

The condenser section has two flanges. The large front flange mates to the bearing-seat flange on the evaporator. They are held together by the previously-mentioned 1/4-inch stud-bolts. A flange at the small end mates to a similar flange on the end plug, through which there are eight 1/8-inch stud-bolts for assembly purposes. The end plug has an extention on its open end that has four 1-inch square surfaces upon which are mounted four phenolic junction boards.

A photograph of the condenser and end plug (with shaft in place) is shown in FIGURE 6.

3.) Auxiliary Equipment

The auxiliary equipment are sub-divided into four groups for ease of description. These are: a.) drive assembly, b.) test stand, c.) spray cooling assembly, and d.) safety shields.

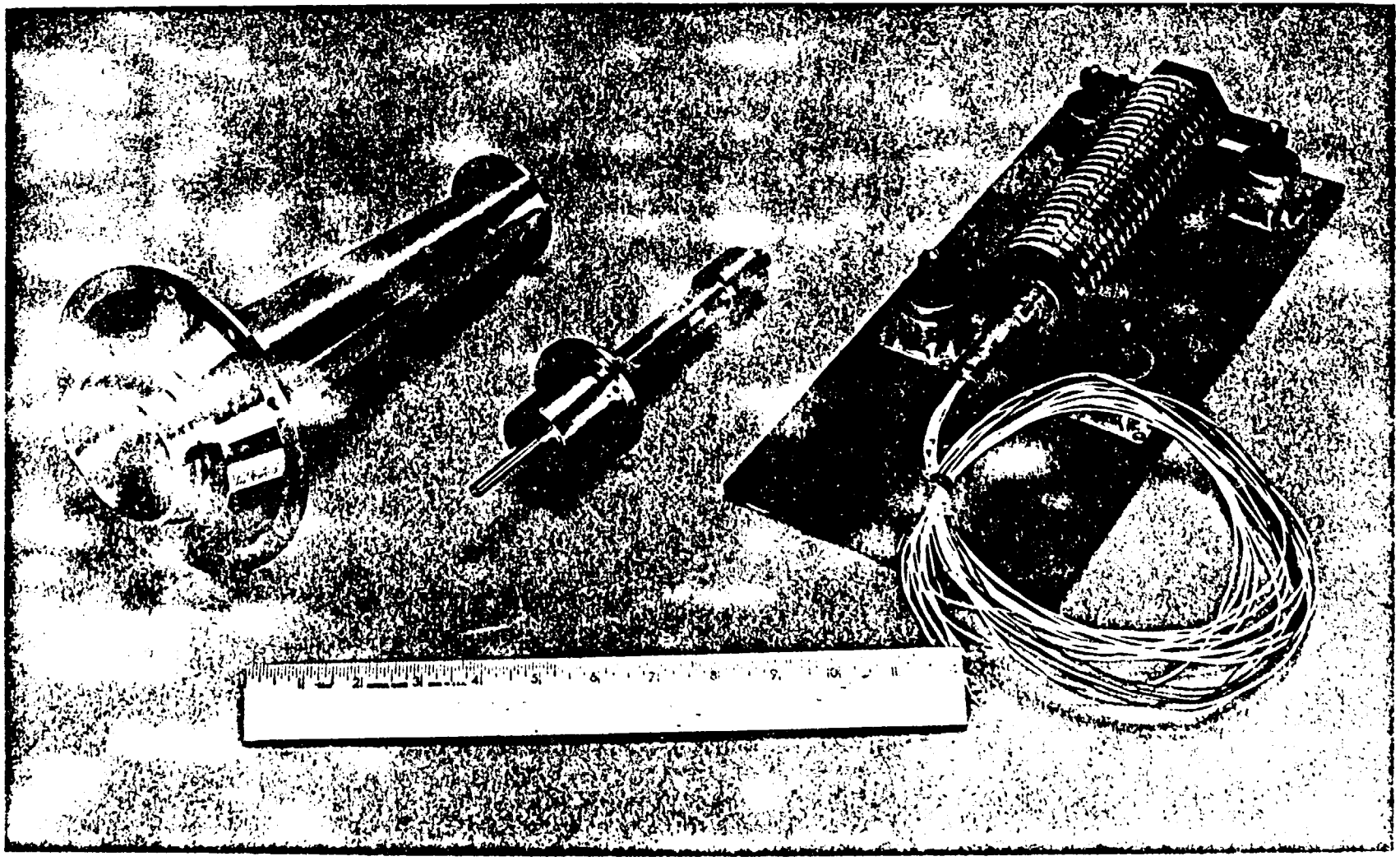

FIGURE 6 Machined Condenser and End Plug (and Slip Ring Unit)

a. Drive Assembly

The drive assembly consists of the end-plug, shaft, pulley, drive motor, and bearing. The end plug has a 3/4-inch threaded shaft way machined into it (See FIGURE 3). Between the shaftway and end of the end plug is a .27 inch hole to allow for the escape of non-condensable gases during filling (to be described later) and for the insertion of a pressure transducer into the vapor space during operation. The shaft is a stainless-steel cylinder which is hollowed to allow the passage of thermocouple leads from the junction boards to a slip-ring unit. The shaft has 3/4-inch of its outside diameter threaded for screwing into the shaftway, and is threaded for 3/8-inch along its inside diameter on both ends. The condenser end holds a $\frac{1}{4}$-inch arm that extends through the hole in the end plug into the vapor space, and into which is screwed a small, semi-conductor pressure transducer, using a teflon-covered thread for sealing. The opposite end of the shaft is threaded to accomodate a coupling to the slip-ring unit that rotates with the pipe.

One-half of a square keyway is machined on the shaft and one-half on the shaftway such that they coincide when the shaft is screwed securely into place in the end plug. A stainless-steel square key is slid into the keyway. The key transmits the rotational torque from the shaft to the heat pipe. The torque is applied to the shaft via a 2.65-inch pulley and v-belt by a 2-horsepower, 3-phase variable speed motor. The motor has a maximum speed of 4500 rpm and a minimum speed of 450 rpm. The speed is controlled by a push-button electric remote control unit. The motor is equipped with a magnetic disc brake for rapid shut-down.

A double row, angular contact bearing is mounted on a seat machined on the shaft. This bearing and the large (5.96-inch inside diameter), floating, single bearing (with bakelite compound cage to withstand high rpm) mounted on the bearing seat on the evaporator flange allow the pipe to easily rotate in any orientation.

b. Test Stand

The test stand was designed to sturdily support the heat pipe assembly mounted on a 15x44-inch steel bed-plate and the motor on its bed-plate. The system operates in orientations ranging from 0 to 90 degrees from the horizontal. Both bed-plates are welded to a 4-inch iron pipe. The pipe is placed in three- 2-inch thick clamps which are supported 2-feet off the ground by $\frac{1}{4}$-inch steel plate. As the pipe is rotated to any orientation, the motor rotates with it and the assembly is then clamped securely in place. Vibrations are kept to a minimum by vibration-mounting the motor. FIGURE 7 is a drawing of a side and front view of the test stand configuration.

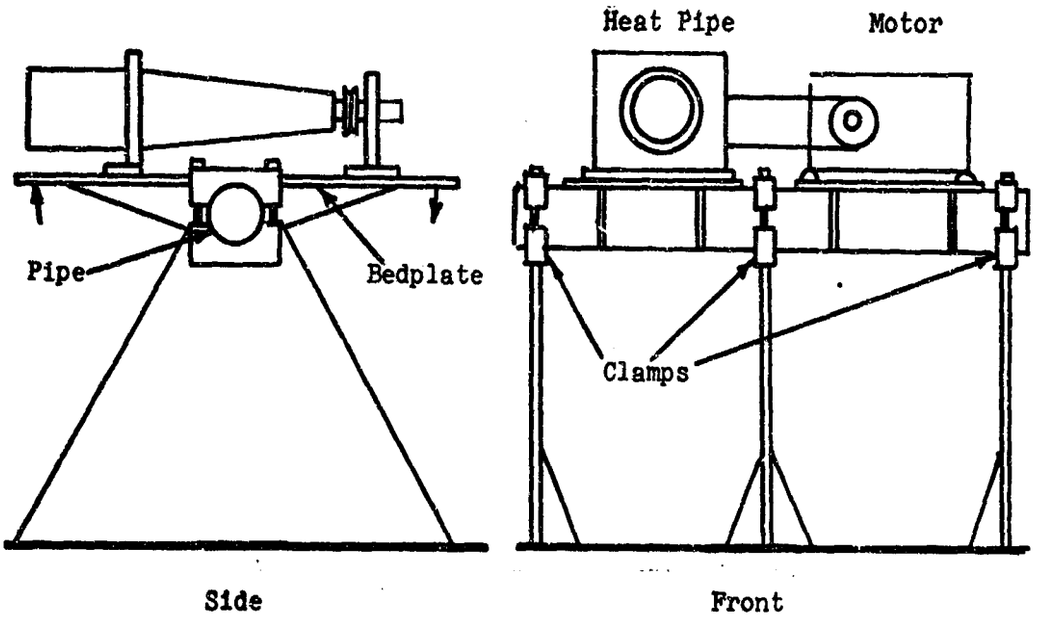

FIGURE 7 Schematic Drawing of Test Stand Configuration

c. Spray Cooling Assembly

The cooling of the condenser section is accomplished by spray cooling. The assembly consists of a cylinder rolled from 1/8-inch thick stainless-steel with an outside diameter of 13-inches that encloses the condenser section. The cylinder is cut in half longitudinally. The bottom half is secured to the bed-plate on which the heat pipe is mounted and the other half is bolted to its mate once the heat pipe is in place and ready for operation. Each half cylinder holds four spray nozzles at the same axial position. The spray nozzles are easily interchanged so that mists of droplets ranging in size from 300 to 600 microns can be obtained. To keep the spray from interfering with the operation of the heater or either of the bearings, 1/8-inch thick shields are welded to the ends of the half cylinders. When the cylinders are mated these shields come within 1/16-inch of the bottom and sides of ridges machined on both the front and rear condenser flanges (see FIGURE 3).

The coolant flows from copper feed lines to a steel mixing tube mounted on top of the spray cylinder. Here the average temperature of the coolant is measured by a quartz thermometer. From the mixing tube the coolant flows through plastic tubing to each of the nozzles. Once sprayed it passes through a drain in the cylinder and bed-plate to a second mixing tube which is also monitored by a quartz thermometer. From here the coolant is sent to an external drain.

d.) Safety Shields

The entire heat pipe is surrounded by 1/8-inch stainless-steel shielding to insure safe operation. The shielding consists

of three components: the evaporator housing, condenser housing, and shaft housing.

The evaporator housing is an inverted-U shaped section that encloses the evaporator. The front end is closed and contains a plexi-glass window to observe internal pipe operation through the pipe viewports. The back end is open and mates with the spray cooling cylinder end shields. The siding has a curved plexiglass window for the visual observance of exterior pipe operation and a door located near the bed-plate for the adjustment of the brush assembly. The inverted-U section slides onto set screws on the bed-plate for easy mounting.

The condenser spray cooling cylinder serves not only as the spray cooling assembly but also as the condenser housing safety shield.

The shaft housing is also shaped like an inverted U and encloses the shaft, pulley, and rear bearing assemblies. Both ends are left open with one sliding against the spray cooling cylinder end shields. A slot is left in the siding for the operation of the v-belt. This section also slides onto set screws on the bed-plate.

4. Instrumentation

The instrumentation is grouped into the following sub-divisions for ease of explanation: a.) temperature measurements, b.) pressure measurements, c.) coolant flow rate measurements, d.) rotational speed measurements, and e.) electrical power measurements. A schematic drawing of the instrumentation setup is shown in FIGURE 2.

a.) Temperature Measurements

Temperature readings are obtained from thermocouples mounted in the evaporator wall to determine a temperature profile and associated heat flux through the wall. Four grounded copper-constantan thermocouples with a 1/16-inch diameter stainless-steel sheath are utilized. They are placed within 1/16-inch diameter wells drilled $3\frac{1}{2}$-inches deep into the stainless-steel evaporator. To insure that no minute air gaps are present between the well walls and the sheaths, a coating of Silver Goop is placed on the thermocouple prior to insertion. Two of the thermocouples are mounted opposite each other at the same radial position to check on the uniformity of the temperature field. This pair is mounted at the middle of the $\frac{1}{4}$-inch wall thickness. The other two thermocouples are also mounted opposite one another, one 1/16-inch radially from the outside evaporator suface, one 1/16-inch radially from the inside surface.

The leads from the thermocouples are brought through both evaporator and forward condenser flanges, down the side of the condenser, and through the rear condenser flange to phenolic junction boards. From the boards the leads go inside the shaft and down to the slip-ring unit which is attached to the main assembly by a coupling mounted at the end of the shaft.

A thermocouple is suspended in the liquid annulus of the evaporator to measure the bulk liquid temperature during operation. A sixth thermocouple is suspended in the vapor space at the evaporator exit to record the saturation temperature of the vapor. The leads to the thermocouples in the liquid and vapor pass through slots in the evaporator

wall (see photograph in FIGURE 4) after passing through the condenser forward flange.

The temperature of the coolant is measured before and after spraying by quartz thermometers mounted in mixing tubes located above and below the condenser spray cooling cylinder.

b.) Pressure Measurements

The saturation pressure of the vapor is measured by a miniature semi-conductor pressure transducer mounted in the vapor space. The transducer is temperature compensated and is threaded on a $\frac{1}{4}$-inch diameter arm that extends from the shaft through the end plug and into the vapor space. The probe's leads pass through the arm, up through the shaft to the junction boards, back into the shaft and down to the slip-rings.

The pressure of the coolant prior to spraying is indicated by a pressure tap on the coolant feed line.

c.) Coolant Flow Rate Measurements

The coolant flow rate is obtained by passing the coolant through a flow rotameter prior to spraying.

d.) Rotational Speed Measurements

The rotational speed of the heat pipe is found by two different methods. First a Hewlett-Packard optical tachometer is employed. Six equally spaced spots mounted circumferentially on the shaft cause the tachometer to emit an electrical impulse each time one passes through its optical field. These impulses are fed to a Donner frequency

counter and counted over a ten second interval. The read-out is in revolutions per minute. The second method of determining the rpm is by the use of an electronic strobe light.

e.) Electrical Power Measurements

The amount of electrical power that the heater is using is found by placing a voltmeter in series and an ammeter in parallel with the power lines returning from the heater.

The power level is controlled by a field rheostat placed in parallel with the DC motor-generator. A 150-ampere circuit breaker is included in the circuit.

A slip-ring unit must be used to obtain readouts from the instrumentation mounted on the rotating heat pipe. A photograph of the slip-ring unit is shown in FIGURE 6. It utilizes liquid mercury as a viscous contact medium between the revolving and stationary leads. This cuts the frictional heating noise to less than 10 microvolts at speeds up to 4000 rpm. The slip ring unit has 22 terminals and is therefore capable of accomodating 9 thermocouples and 1 pressure transducer. The output from the slip-rings is fed to a Hewlett-Packard 2010 C Data Acquisition System containing an integrating digital voltmeter, guarded data amplifier, and guarded cross-bar scanner. This system provides printed digital output with an accuracy of ± 0.5 microvolts.

C. PROPOSED OPERATING PROCEDURES

The operating procedures are divided into three sub-procedures: 1.) filling procedure, 2.) testing procedure, and 3.) treatment of data.

1.) Filling Procedure

Before operating and testing the rotating heat pipe, the working fluid must be introduced into the system. This is done in such a manner as to keep the amount of non-condensable gases in the system to a minimum. These gases reduce the amount of condenser surface available to the vapor. Before filling commences, a maximum operating saturation pressure is decided upon. A limit on the operating pressure is imposed by the amount of pressure the heat pipe is designed to withstand. The maximum operating pressure determines the minimum amount of working fluid that is added to the pipe (the maximum is determined by the amount of liquid the evaporator annulus is capable of holding).

The pipe is placed in a vertical position with the evaporator section down and the shaft not in place. The working fluid is added and a heat flux is generated by passing a current through the heater element. As the liquid evaporates, the vapor drives the non-condensable gases to the end of the condenser and out through the hole in the end plug. Once it is felt that the gases are eliminated from the system, the shaft is screwed into the threaded shaftway in the end plug until it seals against a metallic O-ring located on its end. Heat is still added and liquid evaporated to determine if there is enough working fluid to attain the pre-determined maximum operating saturation pressure. Once this is ascertained, the current to the heater is shut off. The filling phase of operation is completed and testing can commence.

2.) Testing Procedure

Once filling is completed, the test stand is placed in the chosen orientation for the run. Rotation is started and the rpm is

brought to a pre-determined level for the run. This is checked by readings obtained from the optical tachometer and strobe light. The spray cooling system is turned on. Finally, a current is passed through the heater element. The current is increased in steps with a waiting period between each increase to allow the pipe to reach steady-state. The readings of the thermocouples, ammeter, voltmeter, quartz thermometers, pressure transducer, coolant pressure tap, and rotameter are recorded with each current step. This is continued until the maximum saturation pressure level is reached. The same procedure is then repeated for a series of increasing rpm values.

Shut-down is accomplished by first shutting off the current to the heater, then decreasing the rpm by use of the remote control unit (simply turning the motor off will engage the magnetic disc brake). Finally, the coolant system is secured.

3.) Treatment of Data

The amount of heat the heat pipe is transporting during steady-state operation is the primary quantity to be determined from the experimental data. Because of its importance in fixing the operating characteristics of the rotating heat pipe, three methods are used to obtain the heat flux.

The first method is to determine a radial temperature profile in the evaporator wall from the readings of the thermocouples imbedded in the wall. The heat flux is then obtained from Fourier's heat transfer equation in cylindrical coordinates.

The heat flux is also obtained by recording the voltage and current levels to the heater. Once the boiler heat losses are approximated, either by the analytical approach described in Appendix A (using different convection coefficients calculated for different

speed levels) or the experimental procedure described in ref. [6] , the actual heat flux is obtained by subtracting this loss from the gross power input.

The third method for determining the heat flux is by performing an energy balance on the condenser cooling section. The coolant flow rate is obtained from the flow rotameters and from a calibrated curve for the standard nozzles spraying at a fixed pressure, known from the pressure tap reading. The coolant's mean temperature is measured before and after spraying by quartz thermometers mounted in mixing tubes located above and below the spray cooling cylinder. With this information and knowing the coolant's density and specific heat, a heat flux is obtained from a simple energy balance.

The vapor pressure is another important quantity that is monitored during heat pipe operation. It acts as the independent variable in the experimental analysis of the rotating heat pipe. The vapor pressure is determined both from the reading of the pressure transducer in the vapor and the thermocouple mounted in the vapor space. The thermocouple gives an indication of the saturation temperature of the vapor, which can be converted to an equivalent saturation pressure.

The rotational speed is the adjustable parameter in the experimental study of the rotating heat pipe. As indicated previously, its value is obtained by both an optical tachometer and electronic strobe light.

III. ANALYTICAL PROGRAM

A. PRELIMINARY ANALYSIS

In his thesis on the operation of a rotating wickless heat pipe, Ballback [7] discussed the limitations on the rotating pipe due to various fluid dynamic phenomena. Using experimental correlations taken from systems approximating the dynamics of the new heat pipe he was able to estimate the limits of operation imposed by the mechanisms of entrainment, sonic velocity, and critical nucleate boiling. In order to obtain a condenser limit for the conically-shaped condenser section Ballback performed a Nusselt-type analysis for the condensation on a truncated cone. Existing solutions for rotating condensation [8, 9] were not applicable to this geometry since they could not satisfy the condition of zero condensate velocity at the truncated end of the condenser. Ballback's basic assumptions for such an anlysis were justified by classical theory or experimental correlations. With these assumptions and the coordinate system shown in FIGURE 8, he performed force balances in the X-and Y-coordinate directions on an infinitesimal fluid element. After integration and simplification of these basic momentum relationships, an expression for the condensate velocity was obtained.

$$u_f = \frac{\rho_f \omega^2}{\mu_f} \left[\delta Y - \frac{Y^2}{2}\right] \left[(R_o + X\sin\phi - \delta\cos\phi)\left(\sin\phi - \cos\phi \frac{d\delta}{dX}\right)\right] \qquad (1)$$

where
u_f = fluid velocity, (ft/hr)
ρ_f = fluid density (lbm/ft^3)
μ_f = fluid dynamic viscosity, (lbm/ft-hr)
ω = rotational speed (1/hr)
Y = coordinate measuring distance normal to surface, (ft)

δ = condensate film thickness, (ft)
R_o = minimum wall radius in the condenser section, (ft)

ϕ = half-cone angle, (rad)
X = coordinate measuring distance along the surface, (ft)

$\frac{d\delta}{dX}$ = slope of the condensate film

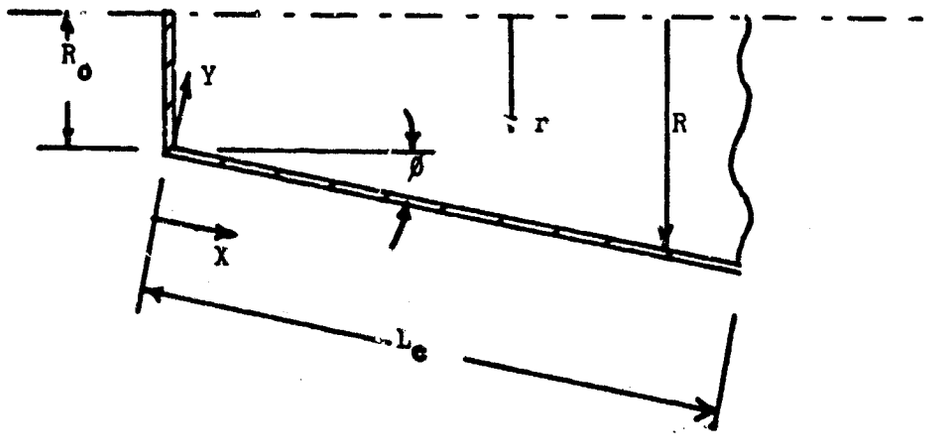

FIGURE 8 Coordinate System for Condensing Limit

From continuity, an expression was obtained for the condensate mass flow rate.

$$\dot{m}_f = \frac{2\pi\rho_f^2\omega^2}{\mu_f}\left[(R_o+X\sin\phi-\delta\cos\phi)(\sin\phi-\cos\phi\frac{d\delta}{dX})\right]\left[\frac{\delta^3}{3}(R_o+X\sin\phi)-\frac{\delta^4}{4}\cos\phi\right] \quad (2)$$

Ballback then assumed that the film is very thin (ie, $\delta \ll R_o$) and that

$$\frac{d\delta}{dX} \ll \tan\phi \quad (3)$$

This assumption allowed the mass flow rate expression, eq'n(2), to be simplified to

$$\dot{m}_f = \frac{2\pi\rho_f^2\omega^2}{\mu_f}\frac{\delta^3}{3}\left[(R_o+X\sin\phi)^2\sin\phi\right] \quad (4)$$

With a steady-state assumption, the rate of condensation equation became

$$h_{fg}\frac{d\dot{m}_f}{dX} = \frac{dq_t}{dX} \quad (5)$$

where h_{fg} = latent heat of vaporization of the working fluid, (Btu/lbm).

$\frac{dQ}{dX}t$ was obtained by considering the heat transfer by conduction to an element of surface area. In determining this expression, Ballback considered only the thermal resistance due to the condensate film and neglected the thermal resistances in the condenser wall and outside cooling mechanism. This simplified expression was substituted in equation (5) which, after integration, yielded a closed-form solution for the condensate film thickness as a function of X. Ballback defined a local heat transfer coefficient as the thermal conductivity of the condensate divided by its thickness. He integrated this expression over the surface of the condenser to obtain a mean heat transfer coefficient. With this mean coefficient a total heat rate for the condenser was derived. Ballback then coupled this condenser heat rate with a conduction equation across the condenser wall to generate a condensing limit curve.

Ballback's results were obtained by neglecting the thermal resistances in the condenser wall and the external condenser cooling mechanism, and by making the additional simplifying assumption that

$$\frac{d\delta}{dX} << \tan\emptyset \quad . \qquad (3)$$

It is apparent that the above assumption, eq'n(3), is true only for large half-cone angles. Also if R_o is zero the mean heat transfer coefficient obtained in Ballback's analysis is identical to coefficient obtained in an existing boundary layer analysis of condensation on a rotating cone performed by Sparrow and Hartnett [9]. They point out that their solution is limited to large half-cone angles.

Ballback's theory can be improved if it is modified to take into account the thermal resistances in the condenser wall and condenser cooling mechanism. This is accomplished by including these terms in the incremental heat conduction equation, which, for a thin condensate film and condenser wall, becomes

$$\frac{dQ}{dX}_t = \frac{2\pi (R_o + X\sin\phi)(T_s - T_{inf})}{\delta/k_f + t/k_w + 1/h} \qquad (6)$$

where k_f = thermal conductivity of the liquid condensate (Btu/hr-ft-^oF)
k_w = thermal conductivity of the stainless-steel condenser wall (Btu/hr-ft-^oF)
t = thickness of condenser wall, (ft)
h = condenser cooling mechanism convection coefficient, (Btu/hr-ft^2-^oF)

When this expression is substituted in the rate of condensation equation (5) along with Ballback's simplified expression for the condensate mass flow rate, a first-order, non-linear differential equation for the condensate film thickness if generated. A closed-form analytical solution for δ cannot be obtained from this formulation. A Runge-Kutta-Gill numerical integration scheme was therefore used to solve eq'ns(4), (5) and (6) using an IBM - 360 Model 67 digital computer and Ballback's heat pipe dimensions. A zero initial condensate film thickness was assumed to start the integration scheme since this is the only value that gives a zero condensate velocity at the truncated end of the condenser. Since this theory is still limited to large half-cone angles by the neglect of the condensate film slope in the mass flow rate expression, the results obtained from the above numerical integration are approximate and are assumed to represent an upper limit on the condensing limit for rotating heat pipe operation.

The condenser limit heat transfer rates are plotted versus rotational speed for a saturation temperature of 212°F and half-cone angles of one- and two-degrees in FIGURES 9 and 10. The outside convection coefficient is a parameter showing the dependence of the heat transfer on the condenser surface cooling mechanism. With an infinite convection coefficient and a 3° half-cone angle, a comparison between Ballback's predicted condensing limit and the condensing limit calculated from the modified theory is shown in FIGURE 11. The modified theory is seen to predict a slightly lower condenser limit heat transfer rate; apparently, neglecting the wall resistance during integration leads to higher rates of heat transfer.

B. REVISED ANALYSIS

The large half-cone angle restriction on the above modified analysis can be removed by including the film thickness slope term in the expression for the condensate mass flow rate.

$$\dot{m}_f = \frac{2\pi \rho_f^2 \omega^2}{\mu_f} \left\{ \left[(R_0 + X\sin\phi - \delta\cos\phi)\ (\sin\phi - \cos\phi \frac{d\delta}{dX}) \right] \left[\frac{\delta^3}{3}(R_0 + X\sin\phi) - \frac{\delta^4}{24}\cos\phi \right] \right\} \qquad (2)$$

When this expression is differentiated and substituted in the rate of condensation equation for steady-state operation eq'n(5), a second-order differential equation for the condensate film thickness is obtained.

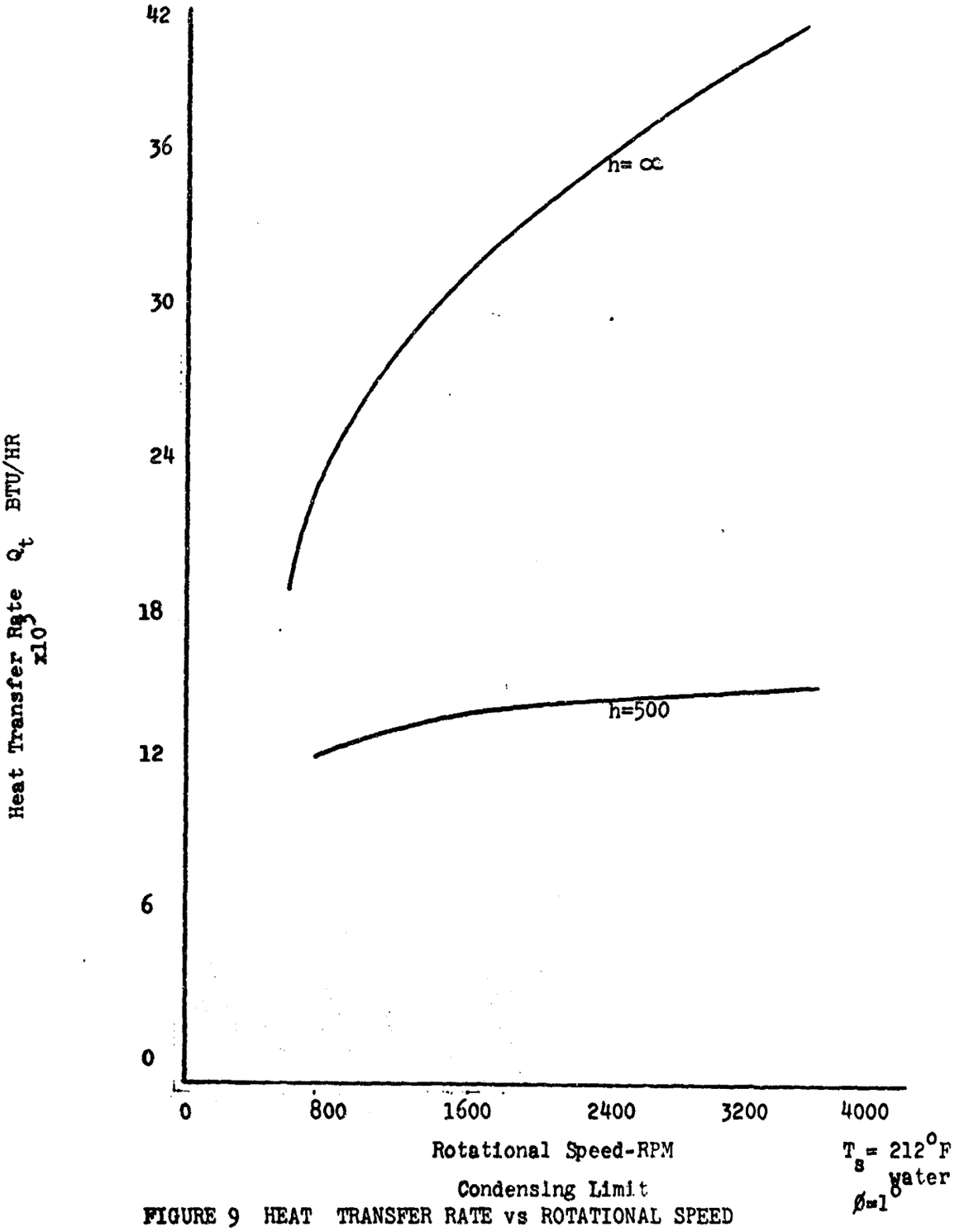

FIGURE 9 HEAT TRANSFER RATE vs ROTATIONAL SPEED

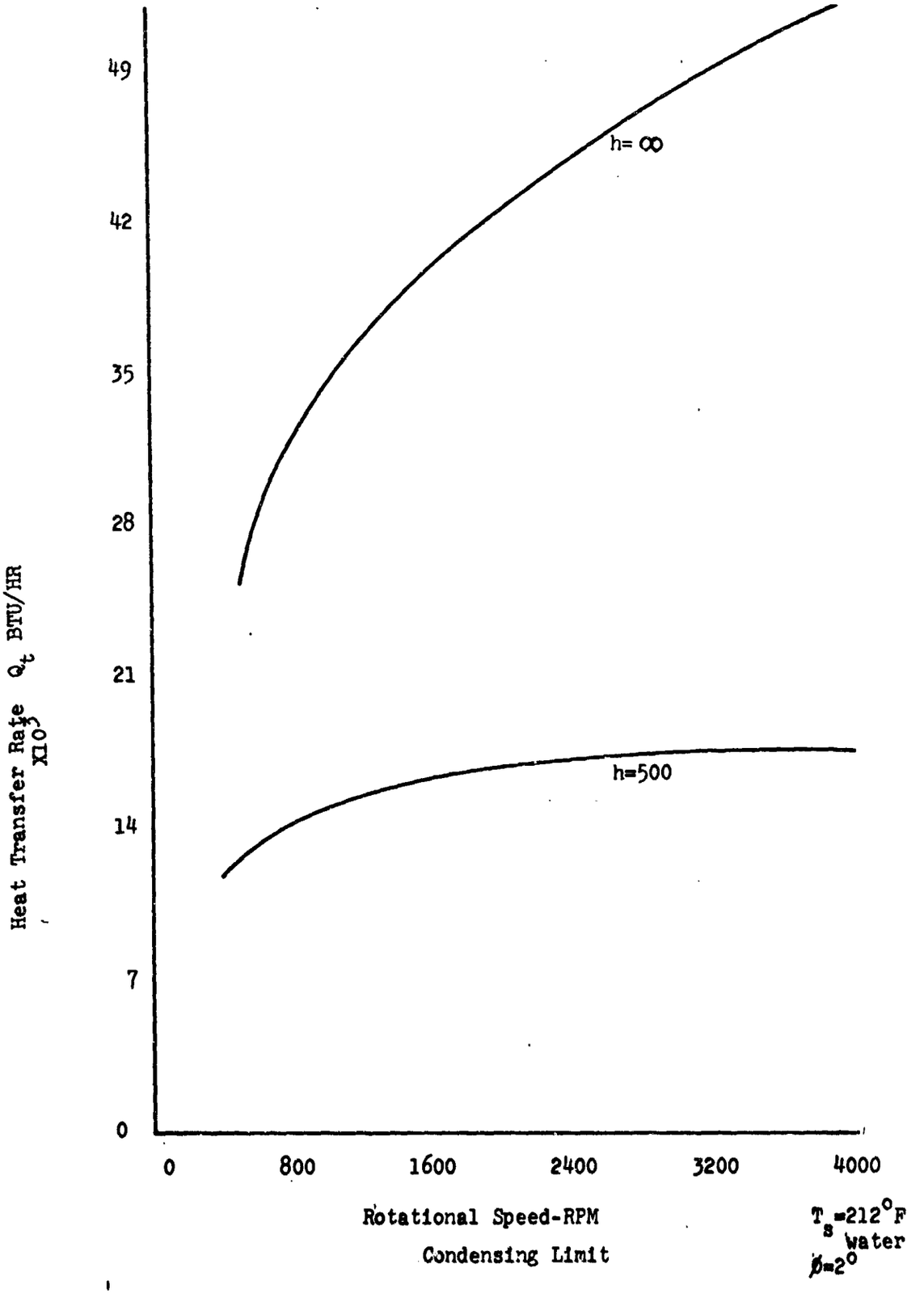

FIGURE 10 Heat Transfer Rate vs Rotational Speed

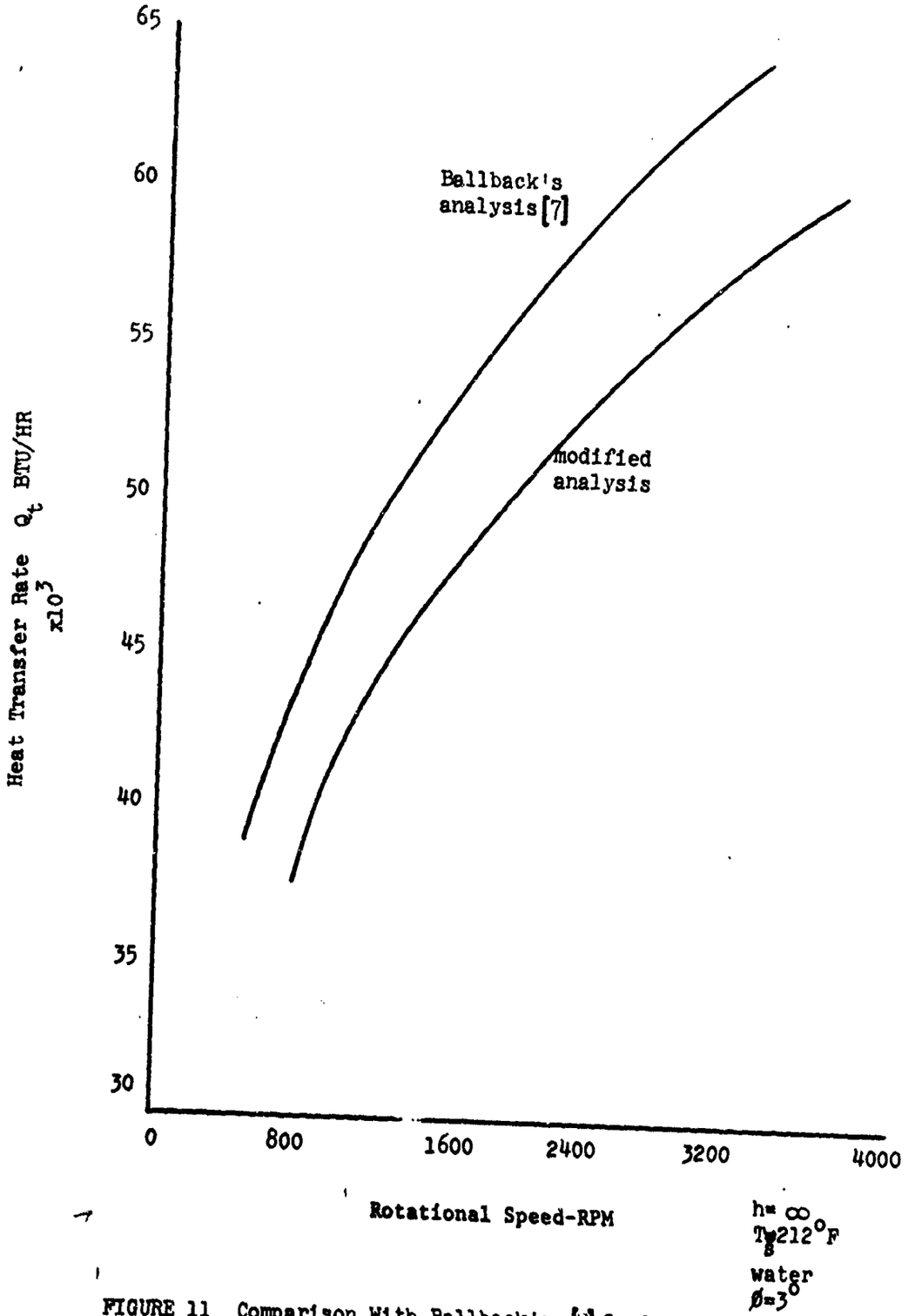

FIGURE 11 Comparison With Ballback's [7] Condensing Limit

$$\frac{2\pi\rho_f^2\omega^2 h_{fg}}{\mu_f}\left\{\left[\sin\phi-\cos\phi\frac{d\delta}{dX}\right]^2\left[\frac{\delta^3}{3}(R_0+X\sin\phi)-\frac{5}{24}\delta^4\cos\phi\right]\right.$$
$$+$$
$$\left[R_0+X\sin\phi-\delta\cos\phi\right]\left[\frac{\delta^3}{3}(R_0+X\sin\phi-\frac{5}{24}\delta^4\cos\phi)\right]\left[-\frac{d^2\delta}{dX^2}\cos\phi\right]$$
$$+$$
$$\left.\left[R_0+X\sin\phi-\delta\cos\phi\right]\left[\sin\phi-\cos\phi\frac{d\delta}{dX}\right]\left[\delta^2\frac{d\delta}{dX}(R_0+X\sin\phi)+\frac{\delta^3}{3}\sin\phi-\frac{5}{6}\delta^3\frac{d\delta}{dX}\cos\phi\right]\right\}$$
$$=\frac{2\pi(R_0+X\sin\phi)(T_s-T_{inf})}{\delta/k_f+t/k_w+1/h} \qquad (7)$$

This expression is valid for all half-cone angles. It reduces upon simplification to existing theoretical expressions for a rotating disc [9] at $\phi=90^\circ$ and for a rotating drum [10] at $\phi=0^\circ$.

A numerical integration method must be utilized to solve equations (6) and (7) simultaneously to obtain a solution for the condensate film thickness as a function of X and the condenser limit heat transfer rate Q_t. To start the integration, initial values for the heat rate, film thickness, and film thickness slope must be determined. Q_t is zero at X=0 since there is no area for heat transfer to occur (the truncated base is assumed to be adiabatic). Leppert and Nimmo [10] state that for condensation on finite surfaces normal to inertial forces, the starting condensate film thickness is a function of the minimum film thickness, which occurs at (or very near) the surface's edge. This is shown in FIGURE 12.

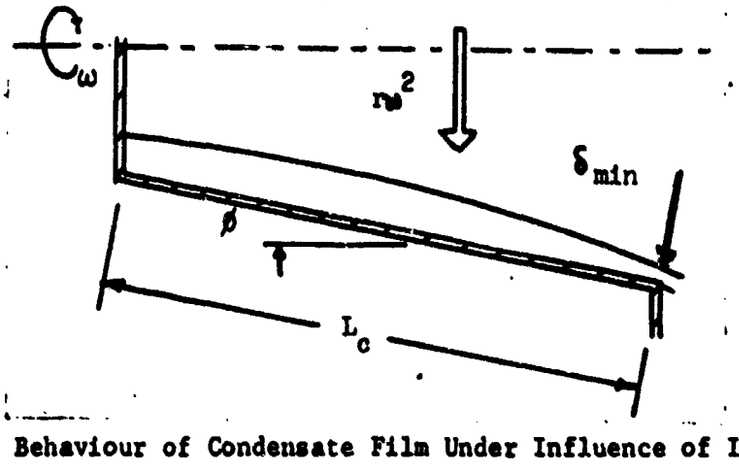

FIGURE 12 Behaviour of Condensate Film Under Influence of Inertial Forces

The minimum thickness depends on the particular overfall condition occurring at the surface's edge. Clifton and Chapman[12] use a free-overfall edge condition to analyze natural convection on a finite horizontal plate. If density variations are replaced by rotational acceleration as a driving force, an expression can be obtained for the minimum condensate film thickness using a free-overfall edge condition. This analysis is outlined in Appendix C with the result that

$$\delta_c = \sqrt[3]{\frac{0.7\,\dot{m}_f^2}{\rho_f^2 (2\pi)^2 (R_0 + L_c \sin\phi)^3 \omega^2}} \qquad (8)$$

where δ_c = condensate film thickness at the overfall, $X = L_c$. From equation (1) in order for the condensate velocity to be zero at the truncated end of the condenser section, the slope of the condensate film must initially equal the tangent of the half-cone angle.

$$\frac{d\delta}{dX} = \tan\phi \qquad (9)$$

The method of solution of the differential equations for the condensate film thickness and condensing limit heat rate resembles that for the solution of a system of non-linear differential equations with an asymptotic boundary condition. With the initial values of the heat rate and condensate slope known, an initial value of the condensate thickness is guessed to start the numerical integration scheme. With these starting values equation (7) is integrated, determining the condensate film thickness as a function of X. The film thickness at $X = L_c$ is compared to that obtained from the free-overfall condition eq'n(8). The overfall thickness is a function

[1] Because of the coordinate system (see FIGURE 8), this is an approximation for all half-cone angles but zero. The exact boundary condition for these angles is not known because the condensate velocity is not zero at X=0

of the condensate mass flow rate at $X=L_c$, which is calculated from equation (2). If the two thicknesses compare, a solution is obtained. If they do not compare, a new guess for the initial film thickness is used as a starting value in the integration scheme. This procedure is repeated until a satisfactory result is arrived at.

A Runge-Kutta-Gill numerical integration scheme was used to solve equations (6) and (7) simultaneously on an IBM 360 Mod 67 digital computer. The initial condensate film thickness was iterated until the final thickness obtained from the integration and that obtained from the overfall condition agreed to within .0004 inches.

Very favorable results were obtained from this procedure for a half-cone angle of zero degrees. However, as the value of the half-cone angle was increased, a problem was encountered which centered about the instability of the highly non-linear second-order differential equation for the condensate film thickness. As is the case with more well-known non-linear differential equations with asymptotic boundary conditions [14] the instability of the equation was highly sensitive to the starting value for the film thickness. Consequently, no numerical results were obtained for half-cone angles greater than zero. The condensing limit heat transfer rate is plotted versus rotational speed for a zero half-cone angle for different values of the outside condenser surface convection coefficient, in FIGURES 13, 14, and 15. The saturation pressure and therefore temperature is a parameter on these graphs. When the thermal resistances in the wall and outside cooling mechanism are neglected, the results compare with those of Leppert and Nimmo [10] for a rotating cylinder.

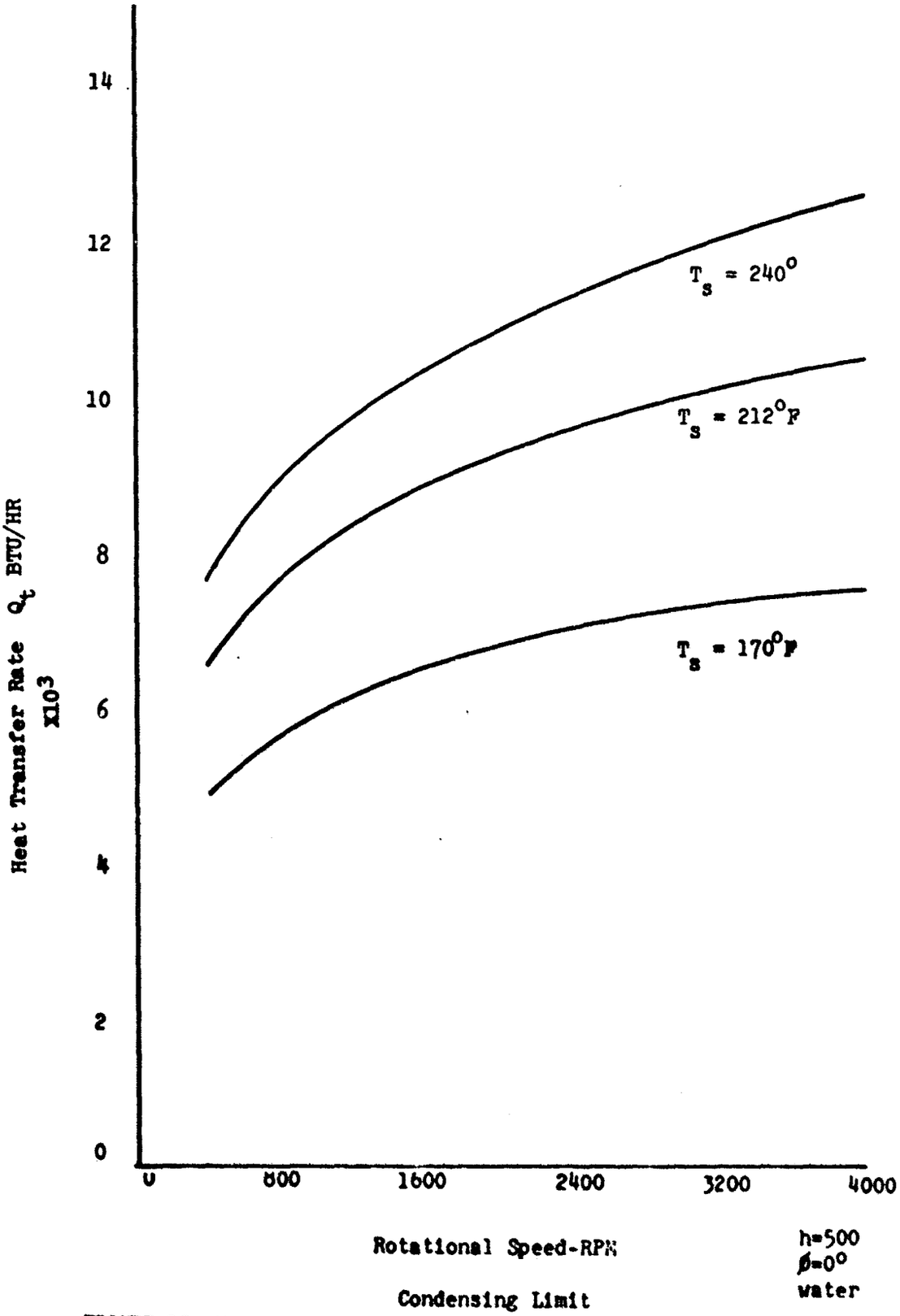

FIGURE 13 Heat Transfer Rate vs Rotational Speed

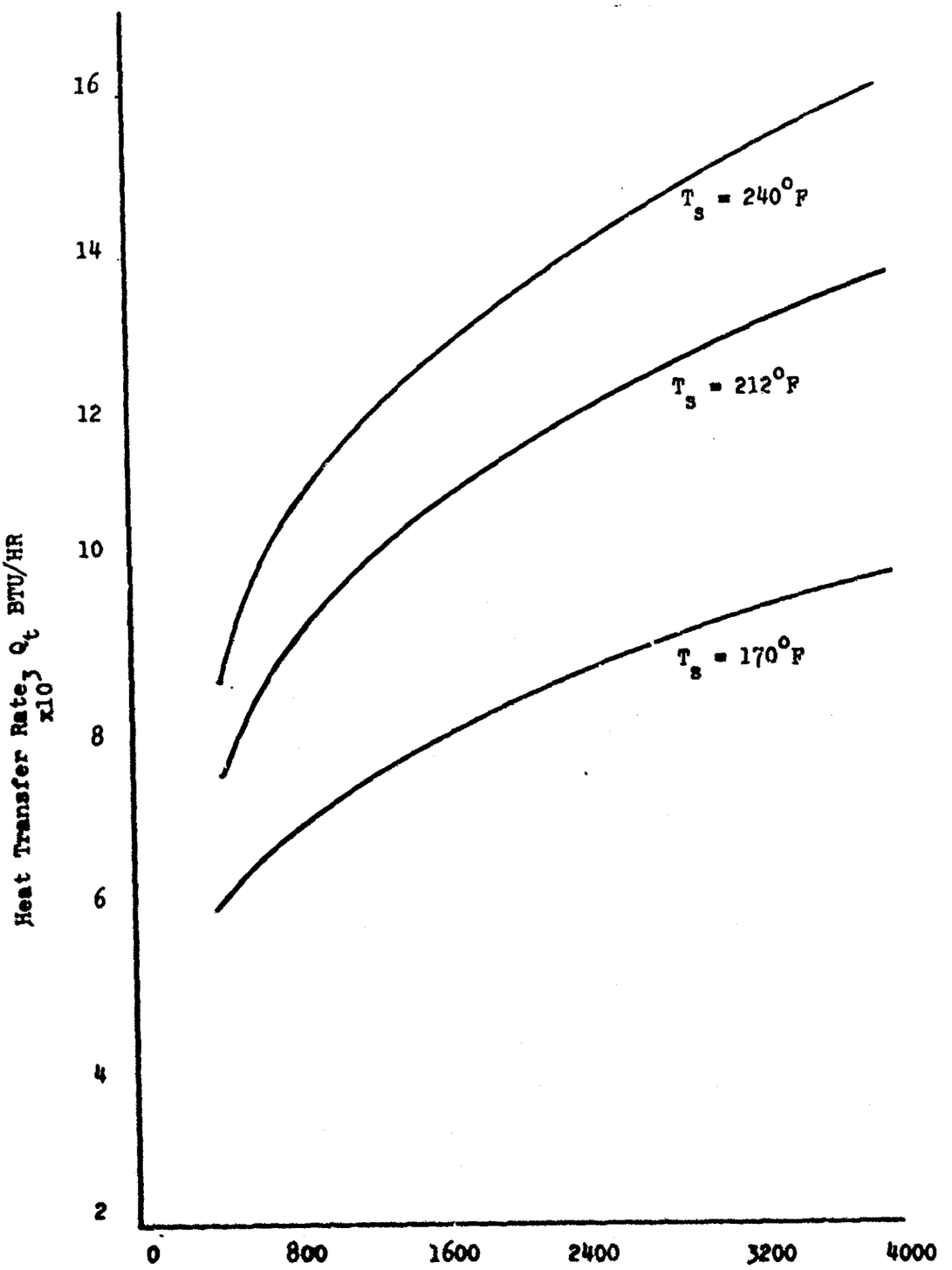

FIGURE 14 Heat Transfer Rate vs Rotational Speed

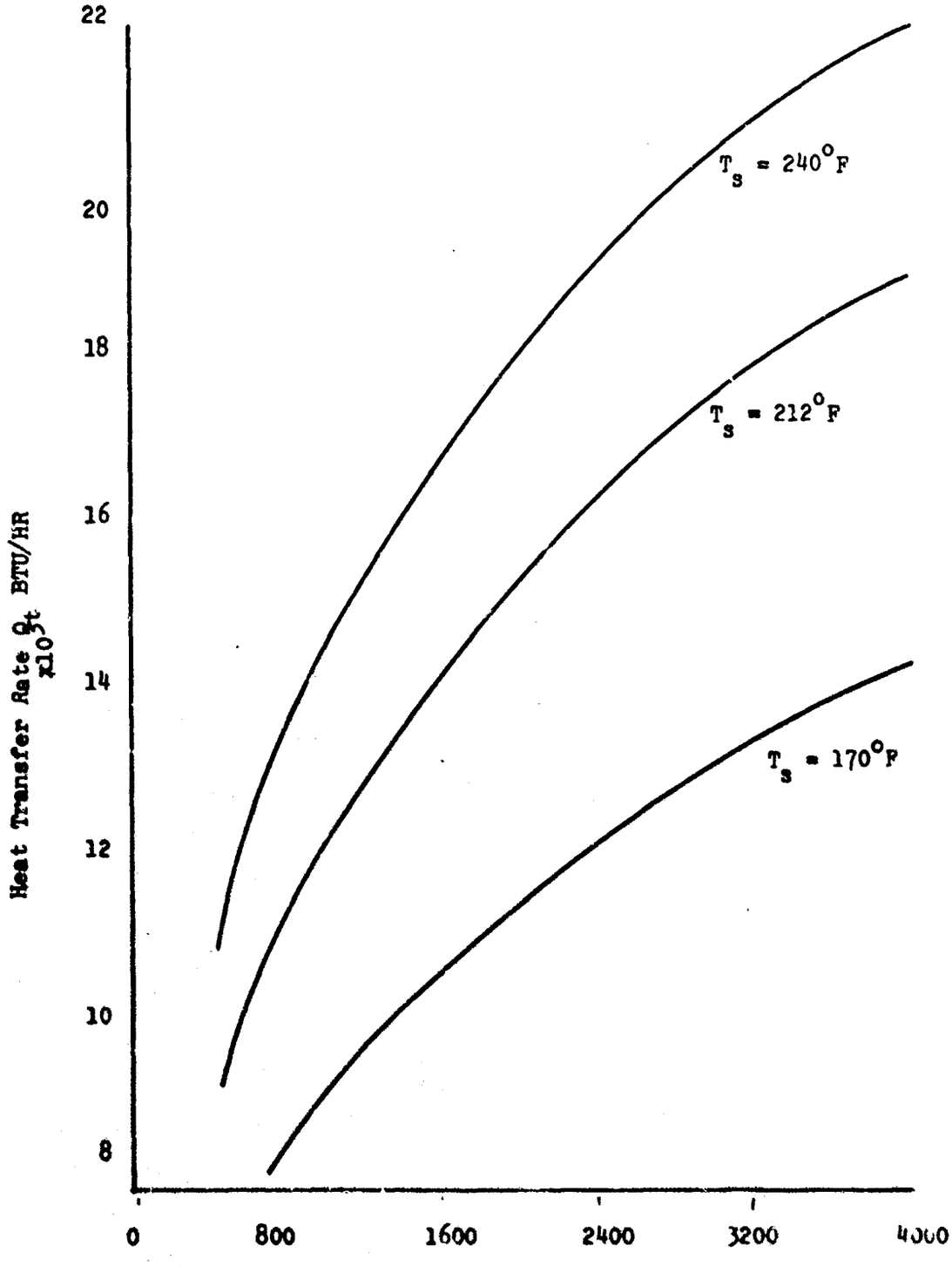

FIGURE 15 Heat Transfer Rate vs Rotational Speed

IV SUMMARY

A. EXPERIMENTAL GEOMETRY

1. The design and machining of the rotating heat pipe has been accomplished as described earlier. It is designed such that visual observations can be made of internal pipe mechanisms such as critical nucleate boiling and condensate entrainment. The instrumentation system is devised so that the parameters of the experimental study such as heat flux, saturation pressure, and rotational speed can be monitored in more than one manner so that checks on a reading can be obtained. A high degree of precision was used in the machining of the pipe and the mounting of the instrumentation to keep the degree of uncertainity in the determination of the operating characteristics to a minimum.

2. The heat pipe and drive assembly are mounted on a special test stand so that tests can be taken on the device at different orientations in the gravity field.

3. Safety is insured during operation by enclosing the rotating assembly within stainless-steel shielding. Plexi-glass viewports and doors in this shielding still allow visual observation of the operation to be accomplished.

B. THEORETICAL STUDY

1. The preliminary theoretical investigation performed by Ballback is limited to large half-cone angles and by the fact that the mean heat transfer coefficient was obtained by considering the effect of the thermal resistance due to only the condensate film and neglecting the effects of the condenser wall and outside cooling mechanism.

2. After amending Ballback's theoretical results to include the thermal resistance effects of the condenser wall and outside cooling mechanism, the condenser limit for a particular operating condition is seen to decrease (i.e., less heat can be removed than was previously expected).

3. Based on Ballback's basic Nusselt-type analysis of condensation on a truncated cone under the influence of rotational forces, an improved theory was obtained that is good for all half-cone angles and includes the effects of thermal resistance in the condenser wall and outside cooling mechanism. This formulation was coupled with a free overfall condition and produced results for a 0^{o} cone angle that are in close agreement with those from existing theory for a rotating cylinder. Results were not obtained for non zero half-cone angles because of the instability of the governing equation, the dependency of this condition being on the accuracy of the initial guess for the film thickness at the truncated end of the condenser section.

4. The condenser limit of the rotating heat pipe is governed by the maximum pressure the pipe is designed to withstand and the amount of working fluid it can contain. If this peak operating level is designed high enough the performance of the pipe may become limited by entrainment or critical nucleate boiling before the condenser limit is approached.

5. The performance of the rotating heat pipe is governed by the method by which the condenser section is cooled.

V. RECOMMENDATIONS

A. EXPERIMENTAL ASPECTS

1. The heat pipe assembly should be completed and the heat transfer capabilities tested for various operating conditions as described in this study.

2. Different condenser geometries should be designed, machined, and tested. Some of the variations could include the varying of the half-cone angle, the addition of some non-wetting material to the condensation surface to promote dropwise rather than film condensation, the machining of longitudinal grooves on the condensing surface to decrease the effect of the interfacial shear on returning condensate, and the placing of fins on the outside condenser surface to increase the effective heat transfer area.

3. Different condenser cooling mechanisms, from air to liquid gases should be utilized and studied.

B. THEORETICAL ASPECTS

1. An iterative scheme such as that described ref. [14] should be formulated and included in the computer program to aid in obtaining theoretical results for half-cone angles other than zero degrees.

2. The effect of the vapor should be included in the theoretical analysis by solving the continuity, momentum and energy equations in the vapor space and coupling this solution with that of the condensate by the common shear stress and temperature at their interface.

APPENDIX A

DETERMINATION OF MAXIMUM RADIAL HEAT FLUX AND ASSOCIATED LOSSES

1. The heater element is made of Chromel A which has a melting point of approximately 2400°F. It is assumed that its maximum surface temperature is 2000°F. Using a cylindrical coordinate system

$$\frac{Q}{L} = 2\pi\Delta\ T/R_t$$

$$R_t = R_{ss} = R_{inc} + R_{MgO}$$

where

R_{ss} = thermal resistance of stainless steel boiler wall (°F-hr-ft/Btu)
R_{inc} = thermal resistance of inconel heater sheath (°F-hr-ft/Btu)
R_{MgO} = thermal resistance of magnesia heater insulation, (°F-hr-ft/Btu)

The resistance of the fluid annulus is neglected due to boiling. From the known geometry of the evaporator section and the known thermal conductivities of the various elements

$$R_{ss} = \frac{\ln\frac{1.8125}{1.5625}}{12} = .01237\ \frac{°F\text{-hr-ft}}{Btu}$$

$$R_{inc} = \frac{\ln\frac{1.8325}{1.8125}}{8.66} = .00127\ \frac{°F\text{-hr-ft}}{Btu}$$

$$R_{MgO} = \frac{\ln\frac{1.8325}{1.8325}}{1.2} = .01275\ \frac{°F\text{-hr-ft}}{Btu}$$

$$R_t = .02638\ \frac{°F\text{-hr-ft}}{Btu}$$

Assuming a maximum operating saturation pressure of 3 atmospheres, the temperature difference across the resistance is

$$T = 2000 - 270 = 1730°F$$

Then

$$\frac{Q}{L} = \frac{2\pi(1730)}{.02638} \cong 420{,}000 \ \frac{\text{Btu}}{\text{hr-ft}}$$

The heating surface is approximately 4 inches long and the boiler inside surface area is

$$A_b = 2 \ (1.5625)\ (4)\ (1/144) = .275 \text{ ft}^2$$

The heat flux is then

$$q = \frac{Q}{A_b} \cong 470{,}000 \ \frac{\text{Btu}}{\text{hr-ft}^2}$$

2. The radial heat losses are calculated in much the same manner. Neglecting the effect of the thin coating of Sauereisen cement, the thermal resistance is

$$R_t = R_{inc} + R_{MgO} + R_{ins} + \frac{1}{hA}$$

where

R_{ins} = thermal resistance of insulation, ($^\circ$F-hr-ft/Btu)
h = outside convection coefficient between the insulation and atmosphere (Btu/hr-$^\circ$F-ft^2)
A = outside surface area of insulation.

It is assumed that the heat transfer on the outside of the rotating evaporator assembly can be approximated by the flow over a stationary cyliner. Then ref. [11] can be used to obtain an estimate for the outside heat transfer coefficient.

$$Nu_D = C(Re_D)^m$$

for $\omega = 3600$ rpm

$$Re_D = \frac{(3600)\ (2\pi)\ (60)\ (d)}{\nu_{air}}$$

where d = diameter of insulation, (ft)

ν_{air} = kinematic viscosity of air (ft^2/hr)

$Re_D \cong 200{,}000$
$C = .0239$
$m = .805$
$Nu_D = 362$
$h = 79$ Btu/hr-$^\circ$F-ft^2
$\frac{1}{hA} = .0277$ $^\circ$F-ft-hr/Btu

$$R_{inc} = \frac{\ln \frac{2.00}{1.98}}{8.66} = .00116 \ ^\circ\text{F-hr-ft/Btu}$$

$$R_{MgO} = \frac{\ln \frac{1.980}{1.952}}{1.2} = .01197 \ ^\circ\text{F-hr-ft/Btu}$$

$$R_{ins} = \frac{\ln \frac{2.75}{2.00}}{.05} = 6.37\ ^{o}\text{F-hr-ft/Btu}$$

These were obtained by assuming a 3/4-inch layer of insulation with a thermal conductivity of .05 Btu/hr-^{o}F-ft.^{2}

$$R_t = 6.41\ ^{o}\text{F-hr-ft/Btu}$$

$$\frac{Q}{L} = \frac{2\pi(1930)}{6.41} = 1890\ \text{Btu/hr-ft}$$

$$q_{loss} = \frac{Q}{A} = 1350\ \text{Btu/hr-ft}^2$$

h can be re-calculated for different rotational speeds, giving a relationship between heat loss and rpm.

3. Using the known evaporator geometry and assuming that 19 helical turns of heater can be wrapped on the 4-inch heating surface, the total length of heater is

$$2\pi\ (1.90625)\ (19)/12 \cong 19\ \text{ft}$$

The resistivity of the heater element is known to be .0785 ohms/ft. This fixes the total resistance in the circuit

$$R = (.0785)(19) = 1.4887\ \text{ohms}$$

If the maximum voltage that can be supplied is 220 volts, the current is

$$I = 220/1.4887 = 150\ \text{amperes}$$

The gross power input is therefore

$$P = I^2R = 32.5\ \text{kilowatts}$$

which corresponds to a heat flux of approximately 350,000 Btu/hr-ft^{2}, assuming losses of 10%.

4. It is therefore seen that the total heat flux capable of being conducted across the evaporator wall is limited by the amount of heat that can generated by the heater.

APPENDIX B

PRELIMINARY UNCERTAINTY ANALYSIS

Assume that the heat flux is to be determined at a surface at a radial distance R by the readings of two thermocouples placed at radial positions r_o' and r_i'. The governing equation is

$$q = \frac{Q}{A_R} = \frac{k(T_o - T_i)}{R \ln(r_o'/r_i')}$$

where

T_o = temperature reading obtained at r_o'

T_i = temperature reading obtained at r_i'

A_R = surface area at the radial position R

k = thermal conductivity of material being used

Then $$dq = \frac{\partial q}{\partial k}dk + \frac{\partial q}{\partial T_o}dT_o + \frac{\partial q}{\partial T_i}dT_i + \frac{\partial q}{\partial r_o'}dr_o' + \frac{\partial q}{\partial r_i'}dr_i' + \frac{\partial q}{\partial R}dR$$

From the governing equation

$$\frac{\partial q}{\partial k} = \frac{(T_o - T_i)}{R \ln(r_o'/r_i')} \qquad \frac{\partial q}{\partial T_o} = \frac{k}{R \ln(r_o'/r_i')}$$

$$\frac{\partial q}{\partial T_i} = \frac{k}{R \ln(r_o'/r_i')} \qquad \frac{\partial q}{\partial R} = \frac{-k(T_o - T_i)}{R^2 \ln(r_o'/r_i')}$$

$$\frac{\partial q}{\partial r_o'} = \frac{-k(T_o - T_i)}{r_o' R [\ln(r_o'/r_i')]^2} \qquad \frac{\partial q}{\partial r_i'} = \frac{k(T_o - T_i)}{r_i' R [\ln(r_o'/r_i')]^2}$$

Then it is seen

$$\frac{dq}{q} = \frac{dk}{k} + \frac{dT_o}{(T_o - T_i)} - \frac{dT_i}{(T_o - T_i)} + \frac{dR}{R} - \frac{dr_o'}{r_o' \ln(r_o'/r_i')} + \frac{dr_i'}{r_i' \ln(r_o'/r_i')}$$

If it is assumed that all the uncertainties are additive and that the values of k and R are known with high accuracy, it is seen that the uncertainty in the determination of the heat flux depends on the

uncertainty in the readings of the thermocouples and in their positioning. It is also seen that the farther apart the thermocouples are placed, the larger the value of the temperature difference and the logarithmic terms become and the smaller the effect of their associated uncertainties become.

APPENDIX C

DERIVATION OF FREE OVERFALL END CONDITION

From ref. [13] it is seen that during flow down a mild, inclined slope, critical flow will occur at a sudden change in slope as shown below.

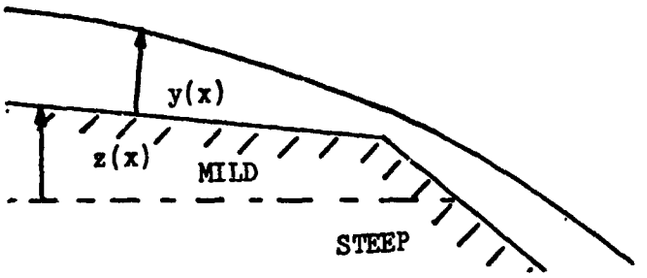

From energy considerations of the system

$$\frac{dy}{dx}\ (1-Fr^2) = S_o - S_f$$

where

$$Fr = \text{Froude Number} = \frac{V}{\sqrt{gy}}$$

$$S_o = \text{bed slope} = -\frac{dz}{dx}$$

$$S_f = \text{friction slope} = \frac{V^2}{c^2 R_s}$$

R_s = wetted mean radius (=A/P)

c = Chezy constant (similar to friction factor, f)

In the region of mild slope, $S_f > S_o$ since the slope is so mild. On the other hand, in the region of steep slope, $S_f < S_o$. Therefore there must exist a point, or region, where $S_f = S_o$. Here

$$\frac{dy}{dx}\ (1-Fr^2) = 0$$

Since the slope of the free surface is not zero, it follows that at this point

$$Fr = 1.0$$

which is the critical condition. Thus,

$$V/\sqrt{gy_c} = 1.0$$

or

$$y_c = V^2/g$$

where y_c is the critical depth.

For flow over a sharp corner, the flow can separate from the steep wall as shown below.

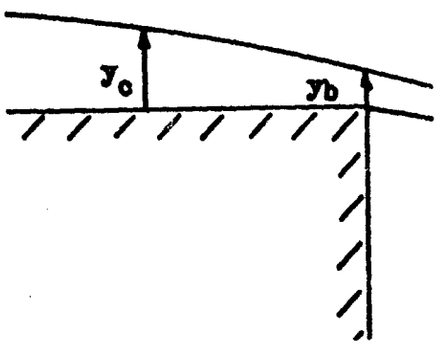

This is called a free overfall. In this case, there is experimental data [15] to show that

$$y_b \cong 0.7 y_c$$

The value of y_c occurs very near the edge of the plate, so that in the case of the condensate film flowing on the condenser wall

$$\delta_c \cong 0.7\, y_c \qquad \text{at } x = L_c$$

where

δ_c = condensate film thickness at the overfall

L_c = the condenser length

$y_c = V^2/g$

Here, V is the average velocity of the condensate given by

$$V = \frac{1}{2\pi R\delta}\int_0^{\delta} 2u_f \pi r \, dy = \frac{\dot{m}_f}{2\pi R \delta \rho_f}$$

where

u_f = velocity of the condensate

$\dot{m}_f$ = condensate mass flow rate

ρ_f = density of the condensate

Also, the acceleration of gravity, g, is replaced by the rotational acceleration term

$$g = \omega^2 R$$
$$\simeq \omega^2 (R_0 + X \sin\phi)$$

where

ω = rotational speed
R_0 = small radius of the condenser cone
ϕ^o = half-cone angle

Therefore,

$$y_c = \frac{\dot{m}_f^2}{\rho_f^2 \omega^2 (R_0 + X \sin\phi)\,(2\pi R\delta)^2}$$

or, at $X = L_c$

$$\delta_c^3 = \frac{0.7\,\dot{m}_f^2}{\rho_f^2 \omega^2 (2\pi)^2 (R_0 + L_c \sin\phi)^3}$$

Finally, as the free overfall condition in the condenser,

$$\delta_c = \sqrt[3]{\frac{0.7\,\dot{m}_f^2}{\rho_f^2 \omega^2 (2\pi)^2 (R_0 + L_c \sin\phi)^3}}$$

BIBLIOGRAPHY

1. Scott-Engineering Sciences, Pub. No. 9068 Heat Pipe Analysis, Design and Experiments by K. T. Feldman, Jr., December 1968.

2. Katzoff, S., Notes on Heat Pipes and Vapor Chambers and their Application to Thermal control of spacecraft. Energy Commission/ Sandia Laboratories Heat Pipe Conference, Vol. 1. October 1966.

3. Mosteller W. L., The Effect of Nucleate Boiling on Heat Pipe Operation, M. S. Thesis, Naval Postgraduate School Monterey California, April 1969.

4. Los Alamos Scientific Laboratory, University of California, Los Alamos, LA-3246- MS. Theory of Heat Pipes, by T. P. Cotter, February 1965.

5. Gray, V. H., The Rotating Heat Pipe - A Wickless, Hollow Shaft for Transferring High Heat Fluxes, paper presented at Eleventh National Heat Transfer Conference, Minneapolis, Minnesota, August 3-6, 1969.

6. National Aeronautics and Space Administration, NASA TN D-4136, Boiling Heat Transfer Coefficients, Interface Behavior, and Vapor Quality in Rotating Boiler Operation to 475 G's, by V. H. Gray, P. J. Marto, and A. W. Joslyn, March 1968.

7. Ballback, L. J. The Operation of a Rotating Wickless Heat Pipe. M. S. Thesis, Naval Postgraduate School, Monterey, California, December 1969.

8. Sparrow E. M. and Hartnett, J. P. "Condensation on a Rotating Cone," Journal of Heat Transfer, Vol. 83. Series C. No. 1, pp. 101-102. February 1961.

9. Sparrow E. M. and Gregg, J. L., "Theory of Rotating Condensation," Journal of Heat Transfer. Series C. Vol. 81, pp. 113-120. May 1959.

10. Leppert, G. and Nimmo, B., "Laminar Film Condensation on Surfaces Normal to Body or Inertia Forces." Journal of Heat Transfer Series C. Vol. , pp. 178-179 February 1968.

11. Chapman A. J. . Heat Transfer, pp. 343-344. MacMillan 1967.

12. Clifton, J. V., and Chapman, A. J., "Natural Convection on a Finite-Size Horizontal Plate," International Journal of Heat and Mass Transfer, Vol. 12, No. 12, pp. 1575-1584. December 1969.

13. Henderson, F. M., Open Channel Flow, pps. 191-202, MacMillan, 1966.

14. National Aeronautics and Space Administration, NASA TN D-3004, Satisfaction of Asymptotic Boundary Conditions in Numerical Solutions of Systems of Non-Linear Equations of Boundary-Layer Type, by P. R. Nachtsheim and P. Swigert, October 1965.

15. H. Rouse, "Discharge Characteristics of the Free Overfall," Civil Engineering, vol. 6, p. 257, April 1936.

Security Classification

DOCUMENT CONTROL DATA - R & D

(Security classification of title, body of abstract and indexing annotation must be entered when the overall report is classified)

1. ORIGINATING ACTIVITY (Corporate author)

Naval Postgraduate School
Monterey, California 93940

2a. REPORT SECURITY CLASSIFICATION
Unclassified

2b. GROUP

3. REPORT TITLE

The Experimental Design and Operation of a Rotating Wickless Heat Pipe

4. DESCRIPTIVE NOTES (Type of report and, inclusive dates)
Master's Thesis; June 1970

5. AUTHOR(S) (First name, middle initial, last name)

Thomas James Daley

6. REPORT DATE	7a. TOTAL NO. OF PAGES	7b. NO. OF REFS
June 1970	60	15

8a. CONTRACT OR GRANT NO.	9a. ORIGINATOR'S REPORT NUMBER(S)
b. PROJECT NO.	
c.	9b. OTHER REPORT NO(S) (Any other numbers that may be assigned this report)
d.	

10. DISTRIBUTION STATEMENT

This document has been approved for public release and sale; its distribution is unlimited.

11. SUPPLEMENTARY NOTES	12. SPONSORING MILITARY ACTIVITY
	Naval Postgraduate School Monterey, California 93940

13. ABSTRACT

An experimental rotating wickless heat pipe apparatus was designed and machined. The apparatus includes a rotating heat pipe assembly, test stand, spray cooling assembly, safety shielding, and instrumentation.

A revised condensing limit for the operation of the rotating heat pipe was obtained by modifying Ballback's Nusselt film condensation theory to include the effects of a thermal resistance in the condenser wall and in the condenser outside surface cooling mechanism. Approximate results, obtained for half-cone angles of 1, 2, and 3 degrees, show that less heat can be removed than originally predicted by Ballback[7], and that the outside heat transfer coefficient can significantly alter the condensing limit.

An improved Nusselt theory was developed which applies for all half-cone angles, and which includes the effects of the thermal resistances in the condenser wall and in the condenser outside surface cooling mechanism. This formulation led to a second-order non-linear differential equation for the film thickness which was numerically integrated using a free-overfall boundary condition at the condenser exit. Results obtained for a half-cone angle of 0 degrees are substantially less than the results obtained from the approximate solution for half-cone angles of 1, 2, and 3 degrees.

DD FORM 1 NOV 68 1473 (PAGE 1)

S/N 0101-807-6811

Security Classification

A-31408

KEY WORDS	LINK A		LINK B		LINK C	
	ROLE	WT	ROLE	WT	ROLE	WT
Heat pipe, rotating						
Heat pipe, wickless						
Film Condensation						

DD FORM 1 NOV 68 1473 (BACK)

S/N 0101-807-6821

Security Classification

A-31409